Desalination 519 (2022) 115221

Contents lists available at ScienceDirect

Desalination

journal homepage: www.elsevier.com/locate/desal

Pilot testing of a novel Multi Effect Distillation (MED) technology for seawater desalination

Shahzada Aly [a], Husnain Manzoor [a], Simjo Simson [a], Ahmed Abotaleb [a], Jenny Lawler [a], Abdel Nasser Mabrouk [a,b,*]

[a] Qatar Environment and Energy Research Institute, Hamad Bin Khalifa University, 34110 Doha, Qatar
[b] College of Science and Engineering, Hamad Bin Khalifa University, Doha, Qatar

HIGHLIGHTS

- Novel design of multi effect distillation
- Installation of 25 m^3/day pilot plant based novel design
- Simulation and pilot testing validate the new design

ARTICLE INFO

Keywords:
Desalination
Multi-Effect Distillation
Pilot plant
Novel evaporator
Techno-economics

ABSTRACT

This work presents an improved evaporator design of the Multi Effect Distillation (MED) to minimize the thermal losses and footprint of the evaporator. An advanced modular MED pilot plant has been installed with a nominal capacity of 25 m^3/day to validate the concept under a seawater salinity of 57,500 ppm (Dukhan Coast, West of Qatar), at the top brine temperature of 65 °C. Both the pilot testing and the simulation results confirm the features of the novel design of the MED. By implementing this invention's design, the heat transfer area has been decreased and accordingly, the capital cost of the evaporator is reduced by 20%. The tube arrangement with new vapor route allows the removal of the traditional demister, which accordingly reduces the footprint of the desalination plant by 65%. The sieve tray for spraying the seawater over the rectangular and inline tube bundle creates a uniform wettability. The improved design also discloses the utilization of an online vent water-ejector, for vent out of the non-condensable gases (NCGs). The novel evaporator design based low temperature MED technology, shows a potential solution for the industrial applications of high salinity byproduct and solar desalination.

1. Introduction

The development of desalination technology is being intensified by the ongoing development of arid regions and freshwater shortage. Desalination technologies, originally developed for the treatment of seawater or brackish ground water can also be modified for the reuse of

Abbreviations: CFD, computational fluid dynamics; GOR, gained output ratio; MED, Multi-Effect Distillation; MED-BD, MED-back side demister; MED-BVB, MED-back vapor box; MED-CT, MED-cross tube; MED-LT, MED-long tube; MED-SD, MED-side demister; MED-SVB, MED-side vapor box; MSF, multi-stage flash; NCGs, non-condensable gases; PLC, programmable logic controller; PR, performance ratio; RO, reverse osmosis; SCADA, supervisory control and data acquisition; SR, salt rejection; TBT, top brine temperature; TDS, total dissolved solids; TVC, thermal vapor compression; VSP, visual simulation program; $T_{seawater}$, inlet seawater temperature to condenser; $P_{seawater}$, inlet seawater pressure to condenser; $T_{f,\,n}$, inlet feed temperature; $P_{f,\,n}$, inlet feed pressure; $T_{v,\,n-1}$, inlet vapor temperature; $T_{v,\,n}$, outlet vapor temperature; $P_{v,\,n}$, outlet (saturation) pressure of the evaporator; $T_{v,\,c}$, outlet distillate temperature from condenser; $P_{v,\,c}$, outlet (saturation) pressure of the condenser; $T_{b,\,n}$, outlet brine temperature; $T_{b,\,n-1}$, inlet brine temperature; $P_{b,\,n-1}$, inlet brine pressure; V_n, outlet (generated) vapor flow rate; V_{n-1}, inlet vapor; $P_{v,\,n-1}$, inlet vapor pressure; D_n, inlet Distillate; $T_{d,\,n}$, outlet distillate temperature; $P_{d,\,n}$, outlet distillate pressure; D_c, outlet distillate flow rate from the condenser; $W_{f,\,n}$, inlet feed; $S_{f,\,n}$, inlet salt; $W_{b,\,n}$, outlet water flow; $S_{b,\,n}$, outlet salt flow; $W_{b,\,n-1}$, inlet water flow; $S_{b,\,n-1}$, inlet salt flow; W_c, cooling seawater reject flow rate; S_c, outlet brine salt flow rate from condenser; δ, boiling point elevation; $\Delta T_{terminal}$, terminal temperature difference.

* Corresponding author at: Qatar Environment and Energy Research Institute, Hamad Bin Khalifa University, 34110 Doha, Qatar.
E-mail address: aaboukhlewa@hbku.edu.qa (A.N. Mabrouk).

https://doi.org/10.1016/j.desal.2021.115221
Received 30 April 2021; Received in revised form 25 June 2021; Accepted 25 June 2021
Available online 4 September 2021

wastewater, for the treatment of industrial effluents and for the preparation of ultrapure water. The large-scale purification of saline water is no longer a question of technological feasibility but of economics. Thus, research and development are aimed at reducing the energy consumption and capital investment requirements of the desalination technologies. Several saline water conversion methods are being practiced on large-scale, while others are in the stage of rapid development. Today, the two most common commercial desalination technologies employed worldwide are membrane- and thermal-based. Presently, desalination caters for roughly 1% of the global drinking water. As of 2020, the number of installed desalination plants worldwide surpassed 20,000 units [1]. In Gulf Cooperation Council (GCC) countries, thermal technology account for 56% of the installed plants, while RO grasped the remaining. In Qatar, however, predominantly employs thermal desalination in 65% of the market, while RO taking 35% of the share [2].

The least exergy required for salt water separation using membrane and thermal concepts, under the same process recovery ratio, showed the same value of specific energy consumption which should be identical in nature [3]. Currently, the RO technology showed a lower specific energy consumption due to the use of an efficient energy recovery system however, the thermal desalination processes have not yet deployed an efficient thermal energy recovery system. Till recent times, most of the thermal desalination R&D focus has been evolving on increasing the unit evaporator size (20 MIGD per unit MSF evaporator and 15 MIGD per unit MED evaporator) to reduce the capital cost. However, there has been little research attention paid to the development of an efficient energy recovery system to reduce thermal energy consumption. The thermal desalination technologies can be much cheaper if abundant waste heat is available. Therefore, thermal desalination units are often installed in the vicinity of fuel-based power plants, often termed as cogeneration in the industry. Comparison between MSF, MED and RO has been showed that the specific energy consumption of all technology regardless type is less when integrated with higher efficiency combined cycle gas turbine power plant however thermal desalination get more advantage due to use a lower exergy of the low-pressure steam. The high Performance Ratio (16–19) MED could be compete with RO, particularly at high salinity water feed [4].

Frantz and Seifert [5] showed that the annual distillate production of a MED unit can be almost doubled if it is operated at 95 °C instead of 65 °C. However, elevated temperatures can expedite the scaling and corrosion, which can drastically increase the downtime of a plant and decrease its service life. In the commercial MED, the evaporation rate influenced by the tube thermal conductivity, tube thickness, and the fluid characteristics. One possibility to increase the evaporation rate is to increase the driving temperature difference, however, the falling film would be affected by the nucleate boiling [6]. The entrainment mechanisms and the critical deflection has been reported [7]. A critical Reynolds number of 300 has been identified to avoid dry patch zone on the heated tube, [8]. The uneven distribution of dripping seawater was simulated to show an uneven scale deposition growth within the tube bundle [9]. Nano–filtration (NF) membrane is proposed to softening the seawater feed of the mechanical vapor compression (MVC) process to work beyond 65 °C up to 100 °C [10]. The photovoltaic (PV) and concentrated parabolic trough (CPT) are proposed to power the NF-MVC system. The economic analysis showed the suitability of a small-scale unit for remote communities.

The MED technology still dominate the brine treatment process to sustain zero liquid discharge applications for the conventional desalination plants brine which usually in the order of 70 g/l. The integrated MED and crystallizer improve the process feasibility in case of selling the fresh water and salt crystals [11]. Nevertheless, thermal separation based supercritical water desalination for zero liquid discharge (ZLD) technology has been examined [12]. The economic evaluation showed the feasibility of the supercritical water desalination brine treatment where all the products were sold. The MED process compete where solar energy and waste heat recovery are available or where the energy is subsidized as the case of GCC countries. An optimized based simulation MED configuration for a small-scale plant has been proposed [13]. The proposed configuration would be cost-effective with at higher thermal energy cost; however, the base configuration (parallel/cross) was cost effective in the case of subsidized thermal energy cost. Falling film collector was proposed to prevent the liquid droplets from bouncing from one to the other tubes which showed an improve of the heat transfer process [14]. CFD analysis of a modified baffle at the bundle sides showed 13% less in the brine carryover [15].

There are several variants of the commercial MED configurations that have been summarized in the previous work of the author [16–18]. Some of these variants are classified according to the vapor box and demister location, while others are classified according to the tube bundle orientation either cross tube or long tube configuration [16–18]. The CFD simulation showed the superior of one configuration to another based on the lower thermal losses due to lower pressure drop within the evaporator. It is a well-known fact that the thermal losses in the vapor route decrease the driving temperature difference which required larger heat transfer to transfer the same heat load. The vapor route resistance become significant at high vapor velocity crossing the tubes. For high-capacity and sizable MED the thermal losses get higher. The existing evaporator design shows a possibility of uneven distribution of the vapor while it is approaching the next tube bundle [16–18]. This is due to the fact that since the vapor released from the previous bundle comes from both sides of the evaporator and it combines in the vapor box at the tail of the tube bundle, vapor vortices are generated due to sudden vapor vector change. Moreover, the tubes which are near to the exit passage receive more vapor than the design value, depriving other tubes of their due vapor quantity. This situation would create imbalance of heat flux in the next tube bundle. As a result, some overheated tubes could exacerbate the scale formation, which is practically unacceptable as scaling hinder the proper heat transfer.

In the falling film evaporator, the feed is sprayed onto the top to bottom tubes, in droplet or column wise as shown in Fig. 1. The generated vapor inside the evaporator must passes through demister, before being directed to the vapor box. In particular, the generated vapor traversing across the tube bundle often causes breakdown of the film of liquid that has shrouded the tubes, which further aggravates the thermal losses. Such film breakdowns can lead to the existence of localized dry zones/patches within the tube bundle. The existence of these dry zones, likely due to unequal distribution of the sprayed seawater feed, degrades the overall performance of falling film evaporator. Moreover, the high vapor velocity across tube bundle will also increase the tendency of seawater droplets entrainment (or carryover) with the vapor. This brine carryover, if not separated properly inside the demister, will yield low quality fresh water.

This work presents a novel design of the evaporator, which not only minimizes the thermal losses but also creates a new vapor route to generate uniform vapor at the entrance of next tube bundle. In this work, a Visual Simulation Program (VSP) code has been developed and validated using a commercial MED-TVC desalination plant (6 MIGD per evaporator, Qatar). The VSP has then utilized to prototype the novel design for the pilot plant. The VSP has been used to perform technoeconomic analysis of commercial plant based novel design and compared with the conventional design. [19]. Typical pilot plant of the novel design has also been installed to verify and validate the concept under different operating and typical seawater conditions.

2. Methodology

2.1. Pilot plant description

Fig. 2 shows a photo of the pilot plant which has been installed in the vicinity of an existing commercial MED plant of Qatar Electricity and Water Company (QEWC), Dukhan, Qatar. The seawater at Dukhan has an average salinity of 57.5 g/L, which is comparatively higher than the

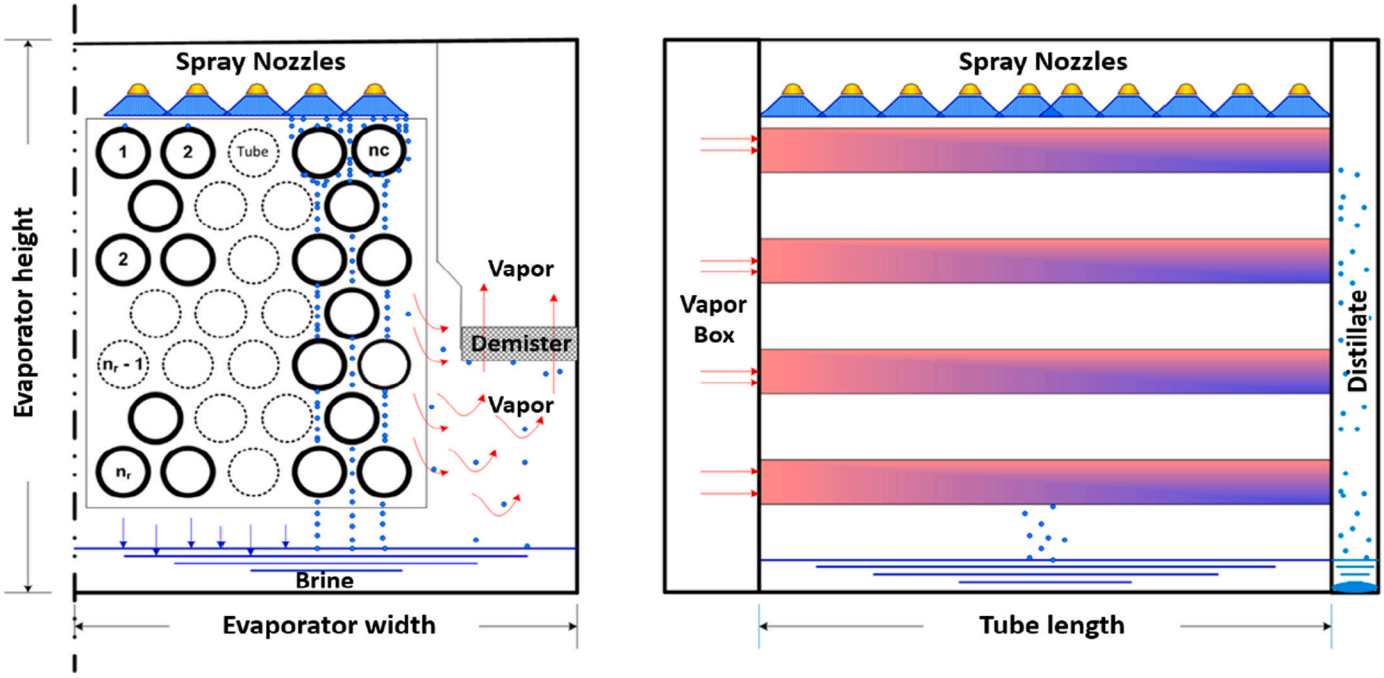

Fig. 1. Cross section of a conventional single tube bundle with spray nozzle for MED evaporator.

Fig. 2. Advance MED pilot plant at the coast of Dukhan, West of Qatar.

average salinity of the oceans (i.e., 33–37 g/L). As can be seen in the block flow diagram of Fig. 3, the pilot plant consists of 3 cells, condenser, two heat exchangers (pre-heaters), and an electrical boiler rated at 350 kW to supply steam to the first cell. The evaporator consists of a single-pass tube bundle that contains 660 tubes per cell. The condenser consists of a three-pass design with 675 tubes (225 tubes per pass) and is designed to condense the vapor generated of the third cell on the shell while the seawater flows through tubes as cooling stream. As shown in Fig. 3, part of T seawater feed (make up) is preheated by splitting and passing part of it through the brine heat exchanger and the rest through the distillate heat exchanger. The hot feed from the brine and distillate heat exchangers is then mixed in feed header and directed towards the three cells. The seawater is fed in parallel with equal amount flow rate to each cell of the evaporator. Each cell is equipped with sieve tray to allow a uniform distribution of the feed onto the tube bundle, which helps in establishing falling film at the surfaces of the

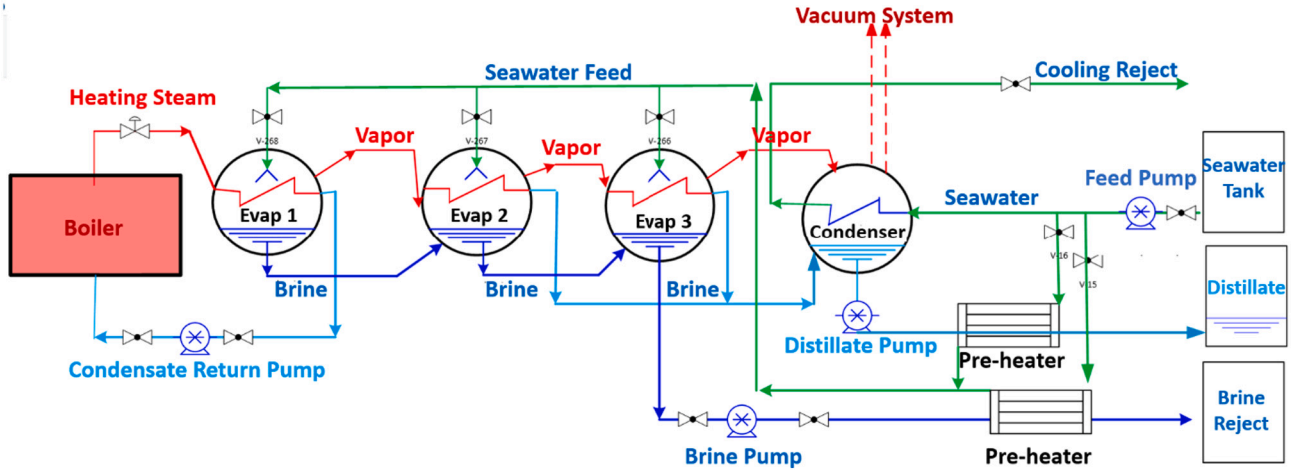

Fig. 3. Block flow diagram of the advanced MED pilot plant.

tube. Vapor generated in cell 1 shell side is directed towards the cell 2 tube side. This vapor condenses within the tubes releasing its latent heat, which is then absorbed by the trickling seawater on the cell 2 shell side. Similarly, vapor generated in cell 2 is directed to cell 3 tube side, where more vapor is generated on the cell 3 shell side. Finally, vapor generated in cell 3 shell side is sent to the condenser, where it is condensed using the cooling seawater supplied at the same temperature as the fresh feed. A water-ejector is used to get rid of the non-condensable gases (NCGs), from all the three cells and the condenser, that are generated during the operation. The water-ejector is also used to create initial vacuum of the

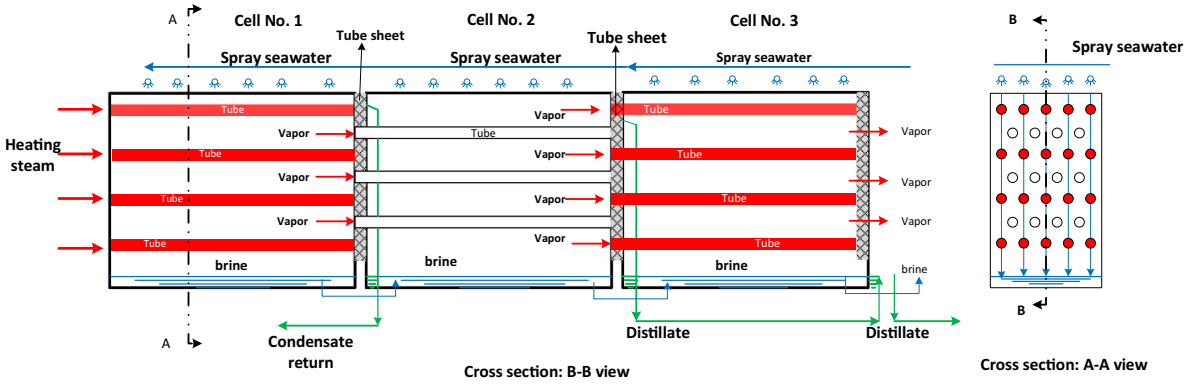

(A)

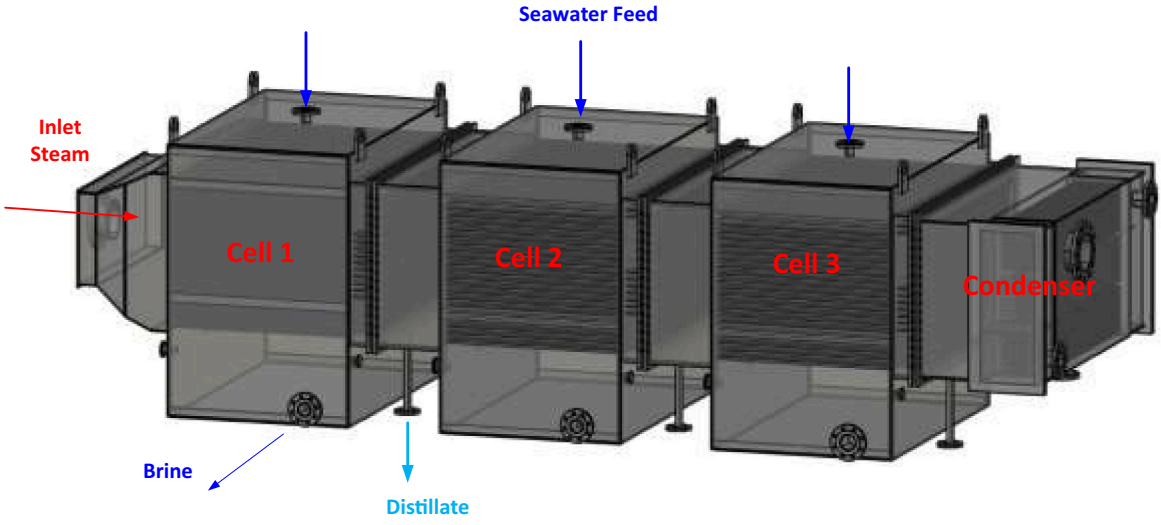

(B)

Fig. 4. (A): A Schematic of the novel design of the evaporator [20] and (B) 3D drawing of the novel design of the evaporator [20].

system, while for deep vacuum a dedicated oil-vacuum pump is employed, capable of attaining vacuum up to 50 mbar. Heat is input into the evaporators in the form of steam, which is generated using the electrical boiler. This steam is fed into the tubes of cell 1 where the condensing steam releases its latent heat energy which is absorbed by the trickling seawater feed on the surface of the tubes and thus, generating vapor. The condensed steam in the cell 1 tubes is sent back to the boiler in a closed loop. Hence, the distillate production considers only the condensation of the generated vapor in cell 2 and 3.

The distillate from cell 2 is sent to the distillate box of cell 3 and then, distillate from cell 3 is sent to the distillate box of the condenser. Eventually total distillate is sent to the distillate tank. Similarly, brine from cell 1 is cascaded to cell 2 and then, the combined brine of cell 1 and cell 2 is sent to cell 3. This is done to promote flashing of the brine in cell 2 and 3, as to further increase the distillate production.

To measure and control various process variables, such as pressure, temperature, flow, levels of brine and distillate, and total dissolved solids (TDS), numerous sensors and actuators were installed. Main actuators are pumps (for feed, brine, and distillate) and the control valves (for steam and feed flow control). To manipulate these actuators, the control logic has been programmed over a dedicated programmable logic controller (PLC), which is further connected to a centralized supervisory control and data acquisition (SCADA) system. The role of the SCADA is to provide overall control, stability, reliability, and safety to the system. All the process variables are recorded on a second-by-second basis and are stored in the SCADA system's server PC installed at the control room.

The proposed design focus on modifying the internal tube bundle arrangement of the evaporator [20,21] to resolve and overcome the issue of the conventional design. As shown in Fig. 4, the generated vapor

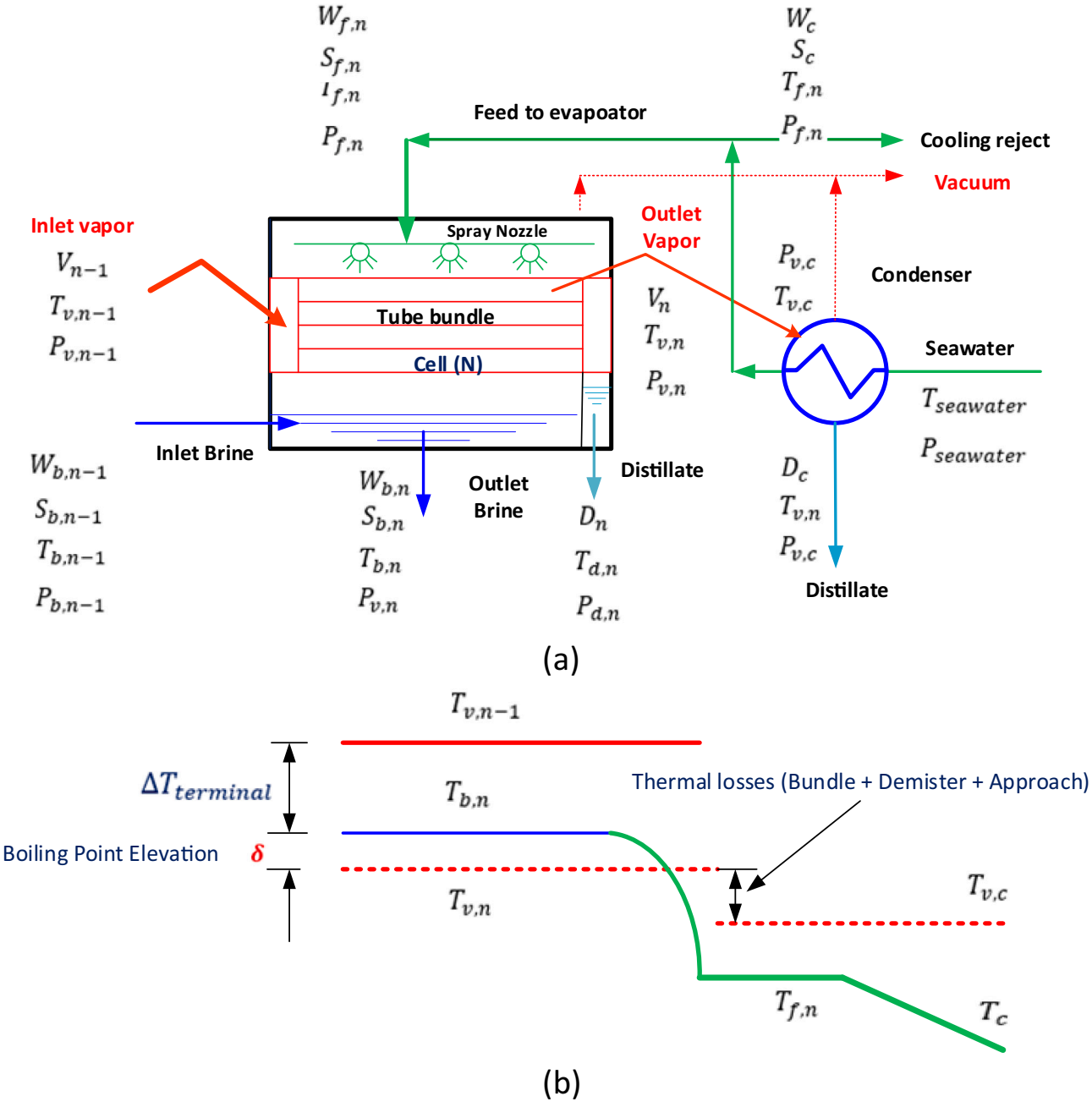

Fig. 5. (A) Process flow diagram and (B) temperature distribution diagram of cell no. (n) and the condenser.

within the tube bundle of the first cell flows parallel to the tubes and passes through the holes in the tube sheet to the tube bundle of the next cell. The tube bundle is arranged to allow the generated vapor to flow in a smooth path without causing much turbulence and to provide the shortest route to reach the next effect. This route is designed to avoid shear losses in between the vapor velocity and falling film. Furthermore, this designed route helps avoid the breakdown of the liquid film around the tubes (i.e., creating dry zones), which in turn does not disrupt the heat transfer process. Since there is no crossflow, this novel route also eliminates the vapor entrainment phenomenon (i.e., brine carry-over). Consequently, there is no need for a demister in this arrangement. Moreover, the novel route also eliminates the vapor boxes, as the generated vapor in the current effect is seamlessly directed to the next effect via holes in the tube sheet. The holes of the tube sheet also make sure that the vapor has a uniform distribution before it enters the next tubes bundle. This eliminates the entrance losses.

2.2. Mathematical modeling

For the detailed techno-economic analysis of the novel evaporator design of advanced MED plant, an in-house developed code has been used. The mathematical modeling details of the developed code and the related process simulation are explained in the sub-sections to follow.

2.2.1. Mathematical modeling of the evaporator

As shown in Fig. 5 (a), for each cell, there are 3 input streams (vapor, feed, and brine from the previous cell) and 3 outlet streams (distillate, brine, and the generated vapor). Each stream is defined with its properties such as pure water flow rate, salt flow rate, temperature, and pressure. The number of unknowns is identified accordingly, and the number of governing equations is presented as follows:

Water balance for cell (n):

$$V_{n-1} + W_{f,n} + W_{b,n-1} = V_n + W_{b,n} + D_n \tag{1}$$

$$V_{n-1} = D_n \tag{2}$$

Salt balance for cell (n):

$$S_{f,n} + S_{b,n-1} = S_{b,n} \tag{3}$$

Heat balance around a single cell (n):

$$V_{n-1}h_{v,n-1} + \left(W_{f,n} + S_{f,n}\right)h_{f,n} + \left(W_{b,n-1} + S_{b,n-1}\right)h_{b,n-1} = V_n h_{v,n} + \left(W_{b,n} + S_{b,n}\right)h_{b,n} + D_n h_{d,n} \tag{4}$$

In a commercial MED evaporator, a demister is used to retain the brine carry over with the generated vapor. However, a pressure drop occurs due to friction losses in the demister. Also, a vapor box is installed between successive effects to collect the generated vapor from the previous evaporator and direct it inside the tubes of the next evaporator. Due to changes in the vapor flow direction, an adequate pressure drop occurs which are converted to thermal loss of the vapor temperature as:

$$T_{v,n} = T_{v,c} + \Delta T_{\text{bundle}} + \Delta T_{\text{demist}} + \Delta T_{\text{vapor box}} \tag{5}$$

Because of the boiling point elevation (δ), the generated vapor temperature will be less than the brine temperature as follows:

$$T_{b,n} = T_{v,n} + \delta \tag{6}$$

At the brine temperature, the boiling point elevation (δ) is calculated using equation [22]:

$$\delta = \left(0.0825431 + 0.0001883 \times T_{b,n} + 0.00000402 \times T_{b,n}^2\right)x + \left(-0.0007625 + 0.0000902 \times T_{b,n} - 0.00000052 \times T_{b,n}^2\right)x^2 + \left(0.0001522 - 0.000003 \times \mathrm{t} + 0.00000003 \times T_{b,n}^2\right)x^3 \tag{7}$$

where, $T_{b,\,n}$ is the brine temperature (°C) and $X_{b,\,n}$ is the average brine salinity (% weight) is estimated to at 90% solubility limit of CaSO4 [22] as below:

$$X_{b,n} = 0.9\left(457628.5 - 11304.11 \times T_{b,n} + 107.5781 \times T_{b,n}^2 - 0.360747 \times T_{b,n}^3\right) \tag{8}$$

As shown in Fig. 5 ('A' and 'B'), the heating steam (V_{n-1}) of the previous cell (n-1) condensed inside the tubes of cell (n), while the seawater is sprayed on the outer the tubes. Due to steam condensation, heat is liberated to boil part of the falling film outside the tubes. The temperature difference ($\Delta T_{terminal}$) between the vapor ($T_{v,\,n-1}$) and the seawater fall ($T_{b,\,n}$) is presented as:

$$\Delta T_{\text{terminal}} = T_{v,n-1} - T_{b,n} \tag{9}$$

The terminal temperature ($\Delta T_{terminal}$) is determined from heating load, the overall heat transfer coefficient (U) and the heating surface area (A) of the tube bundle:

$$V_{n-1}h_{v,n-1} - D_n h_{d,n} = UA\Delta T_{\text{terminal}} \tag{10}$$

The overall heat transfer (U) in Eq. (11) is calculated as:

$$U = 1\Big/\left(\frac{1}{h_i} + \frac{1}{h_o} + \frac{t}{k} + FF\right) \tag{11}$$

And heat transfer area (A),

$$A = n\pi DL \tag{12}$$

where, n, D and L are related to tube number, diameter, and length, respectively.

Also, the pressure of the evaporator ($P_{v,\,n}$) is determined by the thermodynamic balance around the tube bundle.

$$P_{v,n} = \textit{Saturation pressure} \tag{13}$$

$$P_{v,n-1} - P_{D,n} = 0 \tag{14}$$

$$P_{b,n} - P_{v,n} = \varnothing(\delta) \tag{15}$$

$$P_{b,n-1} - P_{b,n} = \varnothing\left(\Delta T_{\text{stage}}\right) \tag{16}$$

$$P_{f,n} - P_{b,n} = \varnothing\left(\Delta T_{\text{subcooling}}\right) \tag{17}$$

$$P_{v,n} - P_{v,n+1} = \varnothing(\Delta T_{\text{loss}}) \tag{18}$$

The details on the variables and the related equations of the mathematical model are provided in [16]. The thermal losses empirical equation of the pressure drops in the demister, vapor box and tube bundle are also presented. The VSP simulator calculates the steam, the chemicals, and the pumping energy. The evaporator capital cost which includes the shell, the tubes are calculated for the reference MED plant [2] which will be compared with novel design evaporator.

2.2.2. Validation of the VSP using process simulation

Overall, each effect will be governed by a set of equations in addition to the equation of state, enthalpies, and correlations [16]. Using the equations described earlier, a well-developed and verified Visual Simulation Program (VSP) [19] simulation code will generate and then solve the governing equations according to the number of effects. The VSP is also capable to predict the performance ratio (PR) of a MED plant with any possible configuration, provided appropriate parameters are defined. For validation, the in-house developed VSP code is used to simulate the Rass Laffan power and water desalination plant at Qatar, which has been taken as a reference for comparison. A low-pressure motive steam of 2.7 bars from a back pressure turbine is used as a heating steam for 10 MED-TVC units. The capacity of each unit is 6.3 million imperial gallons per day (MIGD). The integration of Rass Laffan MED desalination and the power plant is shown in Fig. 6, which is similar in design to the *Al*-Hidd MED plant, Bahrain [23]. The condenser

a.

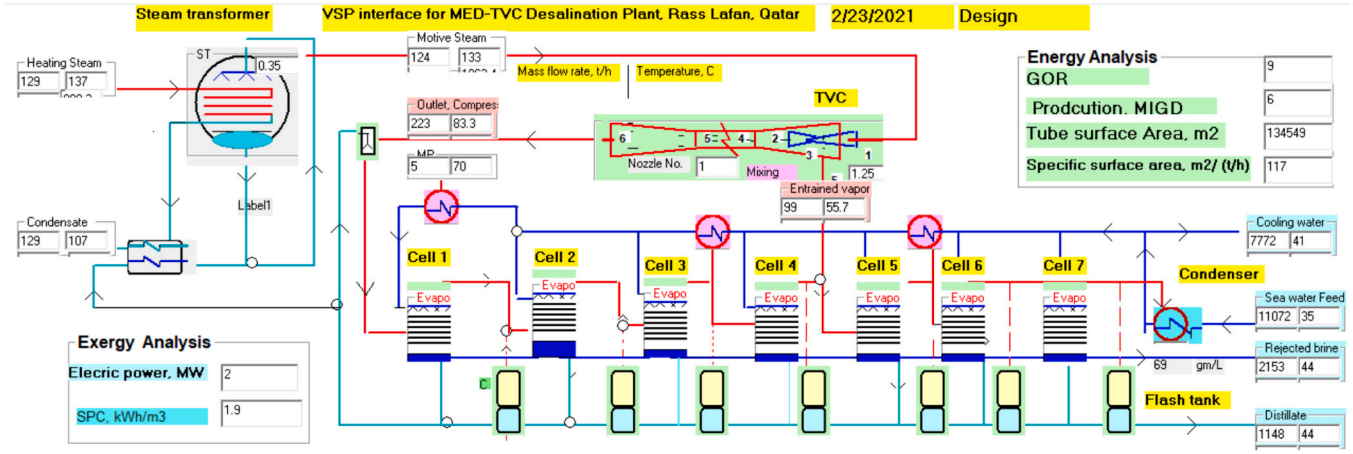

b.

Fig. 6. (A) *Co*-generation power and MED-TVC desalination plant, Ras Laffan, Qatar. (B) VSP software and process flow diagram of Ras Laffan MED Desalination plant (Qatar).

of the power plant is replaced by the steam transformer of the MED desalination plant. The low-pressure steam from the back pressure turbine is condensed in the steam transformer and returned back to the power plant side. The generated steam in the steam transformer is used to run the thermal vapor compression of the MED plant. The electricity to power the pumps of the desalination plant is also provided by the power plant generator. The VSP code is then used to perform process design and simulation of the Rass Laffan MED desalination plant. As shown in Fig. 6, which is the interface of the in-house developed VSP, each unit (total 10 units) consists of 7 effects. The unit capacity, the makeup, and the input steam temperature are specified. The tube length/thickness and the tube material are also specified for the tube bundle. The number of effects is defined. The VSP software calculates the steam consumption, the heat transfer area.

As shown in Table 1, for the reference MED-TVC desalination plant (Ras Laffan), The seawater temperature of 35 °C, Top Brine Temperature (TBT) of 66 °C, motive steam temperature of 137 °C and the unit production of 1148 tons/h are specified as input to the VSP software. The calculated heat transfer area is in acceptable agreement with that of the Ras Laffan MED plant with maximum error of 5%.

Table 1
Validation of the VSP code using Ras Laffan MED plant (Qatar) as a case study.

	Ras Laffan case study	VSP	% diff.
Seawater temperature, °C	35	35	–
TBT, °C	66	66	–
Motive steam temperature, °C	137	137	–
Distillate per unit, ton/h	1148	1148	–
Heat transfer area, Effects 1–4	30,780	32,355	5%
Heat transfer area, Effects 5–7	12,528	12,800	2%

The influence of the vapor entrainment velocity on the falling film deflection evaporators is numerically calculated using the published equation developed by Yung et al. [7].

$$v_{max} = (\varnothing(\varnothing - 1))^{-0.25} \sqrt{\left(\sqrt{\frac{\sigma}{\rho_w g}}\right) 1.575 \frac{\rho_v}{\rho_w}} \quad (19)$$

In this equation the vapor velocity which moves perpendicular to the falling liquid is compared with maximum allowable velocity that avoids entrainment, as shown in Fig. 7.

Table 2 shows a comparison between the maximum allowable vapor velocity to avoid entrainment and the calculated vapor velocity released from the tube bundle for an existing and commercialized MED-TVC desalination plant. The calculated vapor which is released from the bundle is higher than the allowable vapor velocity. The difference varies from 35% at first effect to 40% at the last effect. This indicates that the possibility of entrainment is high during vapor cross over of the liquid film. These results confirmed our hypothesis that changing the vapor route would avoid such possible falling film deflection.

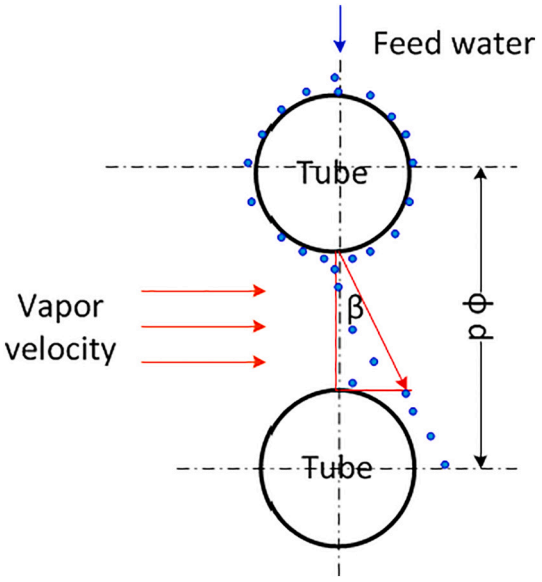

Fig. 7. Influence of the vapor entrainment velocity on the falling film deflection evaporators.

Table 2
Allowable vapor velocities through tube bundle for a commercial MED plant.

Effect no.	1	2	3	4	5	6	7
Allowable velocity, to avoid entrainment	3.9	4.2	4.5	4.9	5.4	5.9	5.8
Vapor velocity through one side bundle	5.3	6.0	7.0	7.0	7.4	6.7	8.1
% of exceeding allowable velocity	35%	42%	54%	45%	38%	14%	40%

3. Results and discussion

3.1. Pilot testing

For this pilot study, the TBT for all the experiments was kept constant at approximately 65 °C and the performance was measured at seawater flowrates varying from 1.00 m^3/h to 3.25 m^3/h per cell. Note that the value 65 °C refers to the TBT of the first cell. The Non-Condensable Gases (NCGs) were extracted using the water-ejector. The timings of extracting the NCGs (for each cell and the condenser) were determined manually by observing the system and understanding the behavior of the control. The condenser pressure for the experiments was set to control the temperature of cell 3, which depends on the vapor pressure.

As an example, for the flowrate of 1.75 m^3/h per cell, different experimental results are presented in Fig. 8, for a minimum of 6 h of steady state operation. The commencement of steady state is defined as the time when the TBT of the first cell stabilizes to a fix value (65 °C in this case), along with the steam consumption and distillate production becoming consistent. The SCADA PLC algorithm is configured to maintain the set TBT of 65 °C by manipulating the steam input and the cooling reject flowrate, along with water-ejector aiding the release of NCGs. Also, as shown in Fig. 8(A) to (C), the system takes almost 5 h to reach steady state in the AUTO mode of SCADA. These results show that the SCADA PLC algorithm provides a good control. On the other hand, the MANUAL mode of SCADA gives full liberty to the operator to control various system parameters such as steam flow rate and cooling reject flow rate etc. However, in this work, all the experiments were performed in AUTO mode, letting the SCADA algorithm decide each and every control action.

Fig. 8(A) presents the total average hourly steam consumption. As can be seen, the steam consumption is consistently around 195.1 kg/h (where the maximum steam producing capacity of the electrical boiler is 200 kg/h once the system reaches steady state. Similarly, Fig. 8(B) presents the temperature profiles for the vapor generated in the three evaporator stages, where the temperature of the evaporator ('Vapor Temp 1') stabilizes to around 67.78 °C (where the given set point was

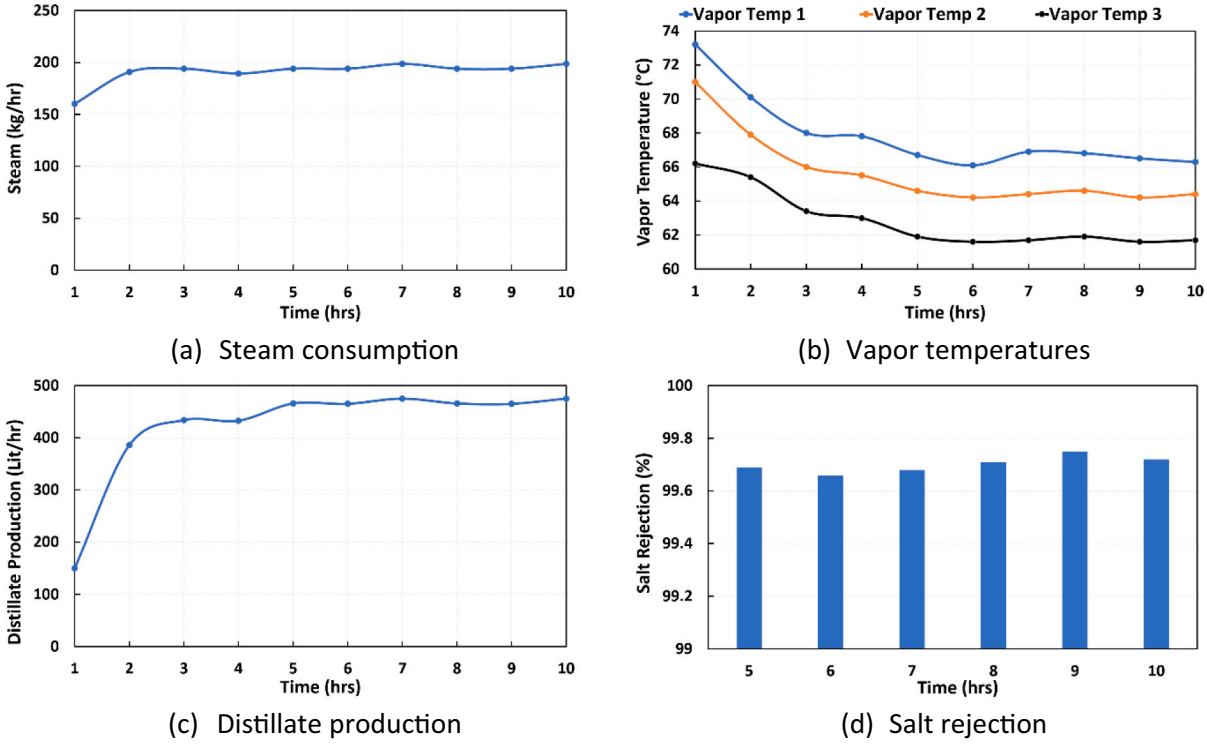

Fig. 8. Various experimental results at a feed flowrate of 1.75 m^3/h per cell at a TBT of 65 °C.

65 °C), after reaching the steady state. As can be seen from the trends of Fig. 8(B), the vapor temperature differences between all of the three stages are approximately 2.5 °C or lower. This successfully demonstrates that the system is working as designed for vapor temperature profiles, where the designed heat loss was approximated to be 3 °C or lower. The extraction timings of the generated NCGs were optimized manually by observing the behavior of the system. Fig. 8(C) presents the total average hourly distillate production. As can be seen, the distillate production varies between 465 and 475 L per hour once the system reaches steady state. Under these conditions, the salt rejection (SR) is calculated for each hour according to equation (20):

$$SR = 1 - (x_p/x_f) \tag{20}$$

The salt rejection shown in Fig. 8(D) is only displayed from hour 5 onwards, when the system reaches steady state. It is lower during the initial transient conditions, where the entrainment of the vapor with seawater/brine is higher due to unsteady and very dynamic conditions of the system. However, the salt rejection improves when the system approaches steady state operation and vapor velocity inside the evaporators becomes stable. The salt rejection calculated for 6 h of steady state operation is around 99.75%, which is acceptable under a high seawater feed salinity of 57,500 ppm (57.5 g/L). The average seawater temperature during this experiment was around 22.3 °C.

3.2. Performance ratio

The performance ratio (*PR*) of MED process is calculated as:

$$PR = \frac{Distillate\ flow\ rate}{Heating\ Steam\ flow\ rate} \tag{21}$$

To simulate the experimental results shown in Fig. 8, a VSP simulation was run at a feed flow rate of 1.75 m^3/h per cell, with set TBT of 67.78 °C, seawater feed salinity of 55 g/L and the seawater temperature of 22 °C (March 2021). Fig. 9 shows the VSP interface for this simulation. The input steam is 200 kg/h to the first effect. The heat transfer area of each effect is given as that of the pilot plant, i.e., 50 m^2 /effect. The condenser surface area and the heat recovery plate type heat exchangers are also defined in the VSP code. The VSP estimates the distillate productivity as 481 L/h and accordingly, the performance ratio to be 2.3. Also, the program calculated the required seawater feed of 12.25 m^3/h, from which about 7 m^3/h is designated for condensing the vapor of cell 3 in the condenser, while the rest 5.25 m^3/h (1.75 m^3/h per cell) is directed to the three evaporators as make up after preheated in the plate type heat exchangers. The TDS of the brine discharged is estimated to be around 62.4 g/L.

For verifying the repeatability of the experiments, the experiment at flowrate of 1.75 m^3/h per cell and at a set TBT of 65 °C (shown in Fig. 10) was performed three times to see the variation of the performance ratio with time. Table 3 shows the variations of different variables for each experiment performed. Here, the average seawater temperature was beyond system's control, while the vapor temperature and the steam consumption were dictated by the SCADA algorithm trying to reach steady state with a TBT of 65 °C. As shown in Fig. 10, for all the three experiments, the steady state performance ratio (PR) was found to be almost the same under the same operating conditions, with average PR for each experiment reported in Table 3. It should be noted that the VSP estimated PR was 2.3, as unlike the real pilot plant experiments variations (shown in Table 3), the VSP assumed all variables to be consistent over time when steady state is achieved. However, the pilot plant results and the VSP estimates are still in a good agreement.

Fig. 11 shows a comparison between simulated and the calculated performance ratio (PR) from the actual pilot tests measured experimental data. The Reynolds number is considered as a dimensionless parameter for base comparison. The Reynolds is calculated function of the feed flow rate (*F*), number of column (*nc*), the pitch (ϕ), the tube length (*L*) and seawater viscosity (μ) as below [9]:

$$Re = 4\acute{\Gamma}_{1/2}/\mu = 2F/[(nc-1)\phi + 1\,]L\mu \tag{22}$$

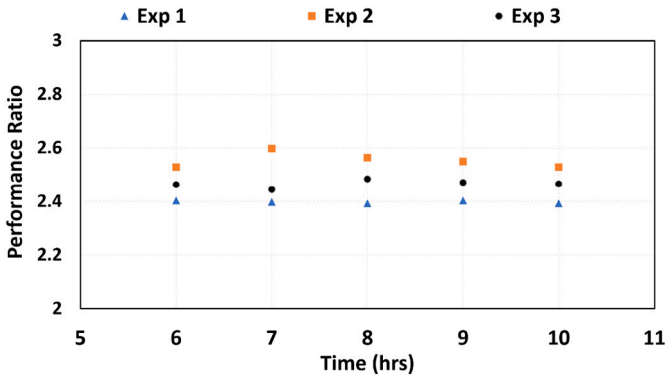

Fig. 10. Replication of the pilot plant production at 1.75 m^3/h flowrate and TBT = 65 °C.

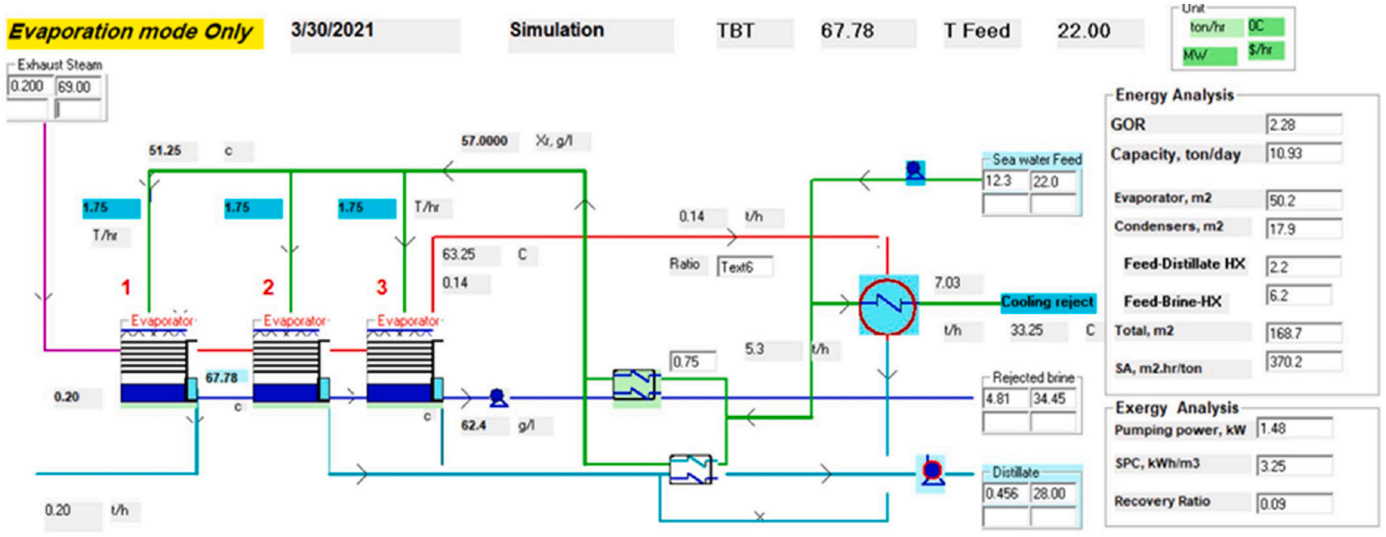

Fig. 9. VSP interface of the pilot plant for performance ratio prediction at a flowrate of 1.75 m^3/h/cell with a TBT of 65 °C.

Table 3
Average values of system variables for different experiments at a flowrate of 1.75 m^3/h/cell with set TBT of 65 °C.

	Vapor temp. (°C)	Seawater temp. (°C)	Steam consumption (kg/h)	Performance ratio
Experiment 1	67.78	21.5	195.1	2.39
Experiment 2	67.71	22.8	198.6	2.55
Experiment 3	66.87	22.1	194.6	2.47

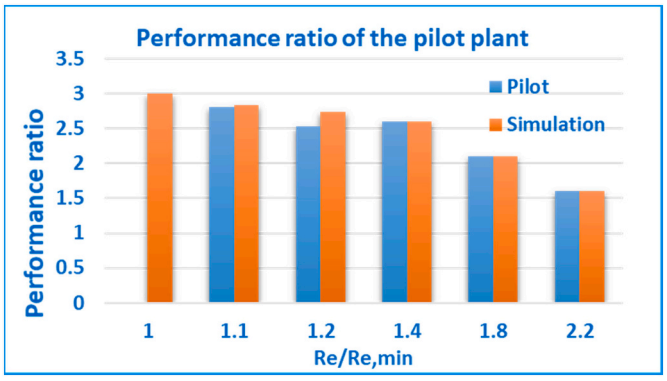

Fig. 11. Comparison between the pilot tests and simulated performance ratio results at different liquid loads.

where, $\acute{\Gamma}_{1/2}$ is liquid load.

To avoid dry patches on the tubes, a minimum Reynolds number is calculated and taken as reference. The minimum Reynolds number was deduced [9] for horizontal tubes with constant heat flux (q) condition as:

$$Re_{min} = q/48 \quad (23)$$

The ratio between the typical Reynolds number from Eq. (22) and the minimum Reynolds number from Eq. (23)are calculated as $\left(\frac{Re}{Re_{min}}\right)$ The ratio of $\frac{Re}{Re_{min}}$ should always exceed 1 to avoid tube dry patches. $\frac{Re}{Re_{min}} = 1$ is the critical condition, and operation of the pilot at this level should be avoided to minimize heavy scale formation on the tubes surface. Fig. 11 shows that as long as the Reynolds number ratio $\left(\frac{Re}{Re_{min}}\right)$ increases, the performance ratio of the pilot plant decreases. This is because of increasing the liquid load which requires more energy to reach boiling temperature. Also, as shown of Fig. 11, there is a good agreement between the simulation and the pilot test results, which confirms the success of the novel design.

3.3. Vapor temperature drop

The vapor temperature drops across the three cells of both novel and conventional design are shown in Fig. 12. The value of the conventional design is calculated from the VSP software while that of the novel design is measured from the pilot plant. As shown in Fig. 12, the temperature drop across the novel design is 20% lower than that of the conventional evaporator. Accordingly, the heat transfer area based on the novel design will be 20% lower than the conventional design, i.e., smaller footprint.

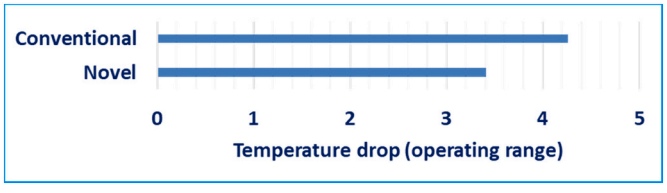

Fig. 12. Temperature drop comparison between the novel and conventional designs.

3.4. Techno-economic analysis

A case study of commercial MED-TVC desalination plant (Qatar) with performance ratio of 9 is considered as reference of comparison. The VSP simulation program is used to perform the simulation under the same operating conditions. Table 4 shows that for the same PR = 9, and the same capacity, the heat transfer area of the novel design is 22% lower than that of the conventional design. This is due to the elimination of the pressure drops in the tube bundle, the demister, and the vapor box. The footprint of the novel design is also 65% lower than that of the conventional design due to the removal of the demister. The cost analysis shown in Table 5 indicates that the tube material cost of the novel design is 24% lower than that of the conventional design. The shell material cost of the novel design is 14% lower than the conventional design. Accordingly, the total evaporator cost of the novel design is 20% lower than that of the conventional design.

4. Conclusions

An advanced Multi-Effect Distillation (MED) pilot plant has been installed based on an in-house design with significant improvements to the traditional process. With a nominal capacity of 25,000 L/day, the new evaporator design has been validated under typical seawater salinity of 57,500 ppm (Dukhan, West coast of Qatar), operating at a top brine temperature (TBT) of 65 °C.

In this study, we focused to validate the new concept under the same TBT, while the seawater feed flowrate in terms of liquid load has been set at varying values. An in-house Visual Simulation Program (VPS) code was also developed and adequately validated to simulate the pilot plant under different scenarios. The proposed design enables elimination of the thermal losses of the MED evaporator, which reduces the total heat transfer area and, accordingly, reduces the total capital cost of the evaporator by 20%. The new tube arrangement of the vapor route enables the elimination of the demister, which accordingly reduces the footprint and the layout of desalination plant by 65%. The advanced MED technology has further features which can be summarized below:

1. The use of a sieve tray for spraying the seawater over the tubes creates a uniform wettability which avoid overheated tubes due to even spray of seawater.
2. Utilization of an online vent water-ejector, for the release of non-condensable gases (NCGs), instead of using traditional jet steam-ejector which requires a high quality (or pressure) steam.
3. The extended tubes of the second effect within the distillate box of the first effect is utilized to condense the remaining in-tube vapor of the first effect while superheating the vapor directed to second effect. The distillate box also enables the collection of the NCGs, from where they can be easily vented by the water-ejector. Accordingly, there is

Table 4
Process parameters comparison between the conventional and novel MED design.

Process analysis	Conventional	Novel MED	Percentage change
Performance ratio (PR)	9	9	–
Specific heat transfer area, m^2/ton/h	171	135	−22%
Footprint, m^2	1152	360	−65%

Table 5
Techno-economic analysis of the conventional and novel MED design.

Process analysis	Conventional	Novel MED	Percentage change
Tube material, M$	18.5	24	−24%
Shell material, M$	6.3	7.3	−14%
Preheaters, M$	0.73	0.75	−3%
Condenser, M$	1.3	1.1	20%
Total (evaporator), M$	33.5	41.8	−20%

no need for a second pass, which simplifies the design in comparison with the conventional design (which uses a second pass of tubes).

- 65% lower in foot print of the novel MED
- Technoeconomic analysis shows 20% reduction in the evaporator cost.

Declaration of competing interest

The authors declare that they have no known competing financial interests or personal relationships that could have appeared to influence the work reported in this paper.

Acknowledgements

1. To Qatar Electricity and Water Company (QEWC), as per 20-Year research collaboration agreement between QEWC and Qatar Environment and Energy Research Institute (QEERI), QEWC already provided a building with all logistics (such as electricity, service water, full access to the seawater intake, and brine outfall facility) for installation of the Multi Effect Distillation (MED) pilot plant. In this building we installed an advanced MED pilot plant and completed phase 1 of project.
2. To the consortium of manufacturing the pilot plant 1. Mubarak Company (Qatar), 2. ESCON Company (Turkey) and 3. AVT company (Turkey).

Appendix A. Supplementary data

Supplementary data to this article can be found online at https://doi.org/10.1016/j.desal.2021.115221.

References

[1] E. Ahmadi, B. McLellan, B. Mohammadi-Ivatloo, T. Tezuka, The role of renewable energy resources in sustainability of water desalination as a potential fresh-water source: an updated review, Sustainability 12 (2020) 5233, https://doi.org/10.1016/j.desal.2007.02.071.
[2] A.N. Mabrouk, H.E.S. Fath, Technoeconomic study of a novel integrated thermal MSF–MED desalination technology, Desalination. 371 (2015) 115–125, https://doi.org/10.1016/j.desal.2015.05.025.
[3] S. Ihm, S. Woo, Comparative study on the methods of calculating theoretical minimum energy requirement for desalination, Desalin. Water Treat. 90 (2017) 32–45, https://doi.org/10.5004/dwt.2017.21018.
[4] S. Ihm, O.Y. Al-Najdi, O.A. Hamed, G. Jun, H. Chung, Energy cost comparison between MSF, MED and SWRO: case studies for dual purpose plants, Desalination. 397 (2016) 116–125, https://doi.org/10.1016/j.desal.2016.06.029.
[5] C. Frantz, B. Seifert, Thermal analysis of a multi effect distillation plant powered by a solar tower plant, Energy Procedia 69 (2015) 1928–1937, https://doi.org/10.1016/j.egypro.2015.03.190.
[6] J. Mitrovic, Preventing formation of dry patches in seawater falling film evaporators, Desalin. Water Treat. 29 (2011) 149–157, https://doi.org/10.5004/dwt.2011.1373.
[7] D. Yung, J.J. Lorenz, E.N. Ganić, Vapor/liquid interaction and entrainment in falling film evaporators, J. Heat Transf. 102 (1980) 20–25. doi:https://doi.org/10.1115/1.3244242.
[8] J.J. Lorenz, D. Yung, Film breakdown and bundle-depth effects in horizontal-tube, falling-film evaporators, J. Heat Transf. 104 (1982) 569–571, https://doi.org/10.1115/1.3245135.
[9] A.A. Mabrouk, K. Bourouni, H.K. Abdulrahim, M. Darwish, A.O. Sharif, Impacts of tube bundle arrangement and feed flow pattern on the scale formation in large capacity MED desalination plants, Desalination. 357 (2015) 275–285, https://doi.org/10.1016/j.desal.2014.11.028.
[10] M.A. Farahat, H.E.S. Fath, I.I. El-Sharkawy, S. Ookawara, M. Ahmed, Energy/exergy analysis of solar driven mechanical vapor compression desalination system with nano-filtration pretreatment, Desalination. 509 (2021) 115078, https://doi.org/10.1016/j.desal.2021.115078.
[11] Q. Chen, M. Burhan, M.W. Shahzad, D. Ybyraiymkul, F.H. Akhtar, Y. Li, K.C. Ng, A zero liquid discharge system integrating multi-effect distillation and evaporative crystallization for desalination brine treatment, Desalination. 502 (2021) 114928, https://doi.org/10.1016/j.desal.2020.114928.
[12] S. van Wyk, A.G.J. van der Ham, S.R.A. Kersten, Potential of supercritical water desalination (SCWD) as zero liquid discharge (ZLD) technology, Desalination. 495 (2020) 114593, https://doi.org/10.1016/j.desal.2020.114593.
[13] A. Liponi, C. Wieland, A. Baccioli, Multi-effect distillation plants for small-scale seawater desalination: thermodynamic and economic improvement, Energy Convers. Manag. 205 (2020) 112337, https://doi.org/10.1016/j.enconman.2019.112337.
[14] T.B. Chang, J.S. Chiou, Spray evaporation heat transfer of R-141b on a horizontal tube bundle, Int. J. Heat Mass Transf. 42 (1999) 1467–1478, https://doi.org/10.1016/S0017-9310(98)00214-2.
[15] M. Khamis Mansour, M.A. Qassem, H. Fath, CFD analysis of vapor flow and design improvement in MED evaporation chamber, Desalin. Water Treat. 56 (2015) 2023–2036, https://doi.org/10.1080/19443994.2014.960460.
[16] A. Mabrouk, A. Abotaleb, CFD analysis of the tube bundle orientation impact on the thermal losses and vapor uniformity within the MED desalination plant, Desalin. Water Treat. 143 (2019) 165–177, https://doi.org/10.5004/dwt.2019.23558.
[17] A. Abotaleb, A. Mabrouk, The impact of vapor box location on the performance of the multiple effect distillation for seawater desalination technology, Desalin. Water Treat. (2021), https://doi.org/10.5004/dwt.2021.26821.
[18] A. Abotaleb, A. Mabrouk, CFD analysis of the demister location impact on the thermal losses and the vapor uniformity within the MED desalination plant, Desalin. Water Treat. (2020), https://doi.org/10.5004/dwt.2020.25222.
[19] A.S. Nafey, H.E.S. Fath, A.A. Mabrouk, A new visual package for design and simulation of desalination processes, Desalination. 194 (2006) 281–296, https://doi.org/10.1016/j.desal.2005.09.032.
[20] A. Mabrouk, Multi Effect Distillation Evaporator, 2016–31325, 2016.
[21] A. Mabrouk, A. Abotaleb, F. Tahir, M. Darwish, R. Aini, M. Koc, A. Abdelrashid, High performance MED desalination plants part I: novel design MED evaporator, in: Proc. IDA 2017 World Congr. Water Reuse Desalin. Water Sci. Sao Paulo, Brazil, 2017: pp. 15–20.
[22] H. El-Dessouky, H. Ettouney, Single-effect thermal vapor-compression desalination process: thermal analysis, Heat Transf. Eng. 20 (1999) 52–68, https://doi.org/10.1080/014576399271583.
[23] Al Hidd, Al Hidd Water Technology, Webpage. (2021). https://www.water-technology.net/projects/hidd/ (accessed April 1, 2021).